Analysis and optimisation of microcrystalline silicon solar cells with periodic sinusoidal textured interfaces by two-dimensional optical simulations

Andrej Čampa,[a] Janez Krč, and Marko Topič
Faculty of Electrical Engineering, University of Ljubljana, Tržaška 25, 1000 Ljubljana, Slovenia

(Received 16 August 2008; accepted 2 March 2009; published online 23 April 2009)

Two-dimensional optical model for simulation of thin-film solar cells with periodical textured interfaces is presented. The model is based on finite element method and uses triangular discrete elements for the structure description. The advantages of the model in comparison to other existing models are highlighted. After validation and verification of the developed simulator, simulations of a microcrystalline silicon solar cell with a sinusoidal grating texture applied to the interfaces are carried out. The analysis and optimization of the two grating parameters—period and height of the grooves—are performed with respect to the maximal short-circuit current density of the cell. Up to 45% increase in the current density is identified for the optimized structure, compared to that of the cell with flat interfaces. Optical losses in the periodically textured silver back reflector are determined. © *2009 American Institute of Physics*. [DOI: 10.1063/1.3115408]

I. INTRODUCTION

Light trapping in thin-film solar cells is important to achieve high absorption of incident light in thin absorber layers.[1–3] Efficient light trapping in the solar cell structures enables to obtain higher conversion efficiencies of the cells and/or gives the possibility for further reduction in the absorber thicknesses. Usually, randomly textured substrates are used to introduce light scattering at the internal interfaces, leading to enhanced light trapping in the cells.[1–3] In order to improve scattering efficiency, other types of textures are of interest—one of them are periodic (diffraction) gratings. Diffraction gratings have a potential for efficient light scattering into large (discrete) angles,[4] giving the possibility for a high level of light confinement inside the absorber layers.

In order to perform detailed analysis and optimization of thin-film solar cell structures with integrated one-dimensional (1D) periodic gratings (lines) at the interfaces, two-dimensional (2D) optical modeling is required. 1D models that assume incoherent propagation of scattered light cannot be used for detailed simulation in this case. In this work we present our 2D optical model that was developed for analysis of thin-film solar cells. The model is based on finite element method (FEM) of solving Maxwell equations. The model was implemented into a user friendly numerical simulator that enables simple analysis and optimization of multilayer structures of solar cells with periodically textured interfaces. The simulator is validated and verified on a simple grating structure and then applied for simulations of a microcrystalline (μc-Si:H) solar cell with 1D gratings at interfaces. The sinusoidal shape of the grating features was optimized with respect to its period (P) and height (h). Potential improvements in short-circuit current density (J_{SC}) of the cell and in absorptance in the intrinsic i-μc-Si:H absorber layer are presented.

[a]Electronic mail: andrej.campa@fe.uni-lj.si.

II. OPTICAL MODEL

A. Theoretical background

Thin-film solar cells are modeled as a multilayer structures with the grating texture applied at the interfaces. The propagation of light is analyzed in terms of electromagnetic waves in the model. The wave equations for the transverse electric (TE) and transverse magnetic (TM) polarization of light are used as presented in Eq. (1). These two differential equations present the basis for determination of the electric (E) and magnetic (H) fields of the light waves at a certain position (element) in the solar cell structure.

$$\left[\frac{\partial}{\partial x}\left(\frac{1}{\mu_r}\frac{\partial}{\partial x}\right)+\frac{\partial}{\partial y}\left(\frac{1}{\mu_r}\frac{\partial}{\partial y}\right)+k_0^2\varepsilon_r\right]E_z=0-\text{TE wave},$$

$$\left[\frac{\partial}{\partial x}\left(\frac{1}{\varepsilon_r}\frac{\partial}{\partial x}\right)+\frac{\partial}{\partial y}\left(\frac{1}{\varepsilon_r}\frac{\partial}{\partial y}\right)+k_0^2\mu_r\right]H_z=0-\text{TM wave}. \tag{1}$$

In the equation the optical properties of media are described by relative permeability (μ_r) and permittivity (ε_r), x, y, and z are the spatial directions, while k_0 is the wavenumber in vacuum and is defined as $\omega\sqrt{\varepsilon_0\mu_0}$ ($\varepsilon_0\approx 8.854\times 10^{-12}$ F/m, $\mu_0=4\pi\times 10^{-7}$ H/m), Z_0 is the impedance of vacuum ($Z_0=\sqrt{\mu_0/\varepsilon_0}$), and ω is the angular frequency.

To solve Eq. (1) numerically, FEM (Ref. 5) is used in our model. For discretization of simulated structures, a mesh of triangular elements is used. The triangular elements are of the same size and orientation. The advantage of the triangular discretization is simpler description (with less elements) of the interface textures of arbitrary shapes, rather than in the case of rectangular elements (most common case in commercially available simulation packages). Because of less simulation points required and especially because they are of the same size (simple matrices formation), calculation time can be decreased significantly.

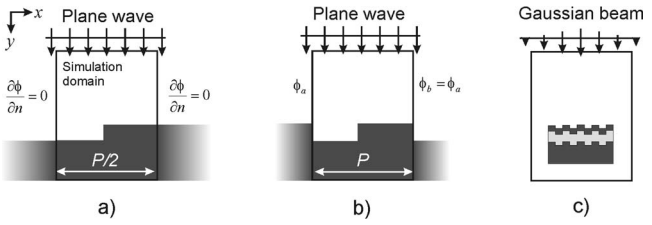

FIG. 1. Boundary conditions at the borders of simulation domain (marked with rectangles): (a) periodic symmetric configuration, (b) general periodic configuration, and (c) open region configuration-bounded system.

The E and H fields (both represented the ϕ symbol in further) inside each discrete triangular element is described either by linear or quadratic approximation:

$$\phi^e(x,y) = a^e + b^e x + c^e y,$$

$$\phi^e(x,y) = a^e + b^e x + c^e y + d^e x^2 + e^e xy + f^e y^2, \quad (2)$$

where e denotes the specific triangular element. The symbols a-f are implicitly determined during the calculation process.[5] The field values at nodes of each element are determined, considering linear or quadratic approximation. For linear approximation each element has three nodes (at each vertices), whereas quadratic approximation has six nodes (at each vertex and at the middle of the edge between two vertices).

B. Boundary conditions

Period of the texture applied to the cell interfaces is much smaller than the cell lateral dimensions. Thus, in the basic case only the region of one (or a half) period can be taken into simulation by considering proper boundary conditions in lateral direction. In the vertical direction, the region (simulation domain) is limited by the thickness of the multilayer structure of the entire solar cell. In Fig. 1, we present three different types of simulation domains (limited to one interface due to simplicity reasons) which are related to different boundary conditions used in our model. In the case of symmetry of periodic structure with respect to the left and right borders of the simulation domain [Fig. 1(a)], the homogeneous Neumann condition is used at the left and right borders (derivative of ϕ in normal direction (n) is zero: $d\phi/dn=0$). In this case only half of the period is taken into simulation, significantly reducing the time of calculation. The second case takes into account the whole period [Fig. 1(b)], and the left and right boundaries have the same ϕ ($\phi_a=\phi_b$). The third condition that can be used in our model [Fig. 1(c)] enables to simulate laterally limited structures (or illuminations). In this case the periodicity is not assumed outside the simulation domain. Absorbing boundary conditions[5] (ABCs) are used, and the propagated field is absorbed in the boundary region (imitating the propagation in the infinite space). This third case enables to simulate the situations, where the periodic gratings are illuminated by laterally limited sources (e.g., a laser source with small spot size). This type of simulation is very important, since it enables direct comparison with the results of scattering characterization of the gratings (determination of haze parameter and angular distribution function of scattered light[6]).

ABC is also applied to the top and bottom borders of simulation domain in all three cases [Figs. 1(a)–1(c)]. At top border additionally to the ABC, the illumination is applied: plane wave in the case of Figs. 1(a) and 1(b) and Gaussian beam (or other) in the case of Fig. 1(c).

In the case of oblique incidence of light on the analyzed structure, the cases of Figs. 1(b) and 1(c) are relevant. Figure 1(a) with its ability of mirroring the electric field and structure over left and right borders is not appropriate. In Fig. 1(b) the left and right boundaries have to be modified to meet the general periodic boundary condition,[7,8] while Fig. 1(c) is self-sufficient and does not need to be modified, only nonperpendicular illumination has to be generated. In this work, simulations and analyses are focused on perpendicular incident illumination only. However, nonperpendicular incident angles of reflected and transmitted scattered light at grating interfaces (multilayer systems) in the structures are taken into account also in this case. If symmetric structures are analyzed and the incident illumination is perpendicular, boundary condition presented in Fig. 1(a) is desirable, since less elements can be used (half period only) in the simulation.

C. Solving the system of equations and determination of output parameters

By considering Eqs. (1) and (2), boundary conditions and the discretization of the simulation domain the system are numerically solved by applying the Ritz method.[9] This method is based on minimization of variational functional. The minimum of functional corresponds to the given differential equation [Eqs. (1) and (2)] and its boundary conditions, which restrain the simulation domain. Minimizing the functional for every element of the simulation domain and combining them together over the whole domain, the system of equations is obtained. The system can be presented in a matrix form $\mathbf{K\Phi=b}$, where $\mathbf{K}$ is a sparse matrix of the system coefficients (the size of $N\times N$, where N is the number of all nodes in the simulation domain), $\mathbf{\Phi}$ is the vector of the system unknowns (E or H, the vector size is N), and $\mathbf{b}$ is the vector of the light sources (the size of N). The number of unknowns can, in realistic cases, reach the order of millions. The system of equations is solved by applying different iterative methods (biconjugate gradient, conjugate gradient, and conjugate gradient squared method).[10,11] To stabilize and improve the convergence, different preconditions are used (e.g., Jacobian and symmetric successive over relaxation[10,11]). To obtain good convergence with accurate solutions of the system, at least 20 unknowns (for linear approximation) per effective wavelength ($\lambda_{\mathrm{eff}}=\lambda_{\mathrm{air}}/N_{\mathrm{layer}}$) has to be taken into account. However, special attention has to be paid when metal layers with high absorption coefficient are simulated. Especially sharp metal edges are problematic for TM polarization, where spikes in the field occur. Based on our analyses, we have to use at least 40 unknowns per effective wavelength to efficiently simulate the field effects related to metal layers.

After the system is iteratively solved, the values of ϕ at each node of the triangular element are available for postpro-

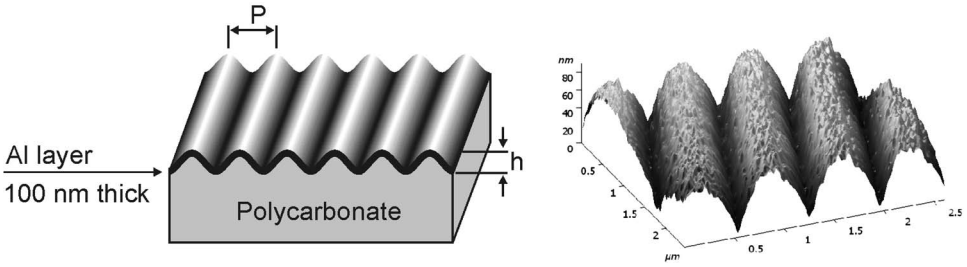

FIG. 2. Schematic view of the analyzed grating structure with a film aluminum layer (100 nm) on top of the polycarbonate substrate (left) and the actual Al surface morphology detected by AFM (right).

cessing. In our analysis, we are interested in obtaining the parameters related to the optical properties of the thin-film solar cells. We have implemented the autocalculation of total reflectance, absorptance in each layer, and the 2D generation rate across the structure of the photogenerated electron and hole pairs in the active layers.[12]

The advantage of the modeling approach described above is very low memory consumption, due to the used sparse matrix for the system coefficient matrix (**K**). Furthermore, the sparse matrix enables very fast calculation of vector-matrix product which presents a bottleneck in the speed of processing. As mentioned, by using triangular elements the arbitrary shapes can be very well defined, with no abrupt steps. The model was implemented in a computer simulator with user friendly interface that enables simple handling of input parameters (multilayer structure, grating parameters, etc.) and output data, which can be easily implemented in a 2D electrical simulator.

D. Verification of the modeling approach on a grating structure

The results of verification are shown for a simple Al covered (d_{Al}=100 nm) grating structure, which was embossed in a polycarbonate substrate (Fig. 2, left side). The morphology parameters of the grating were determined by atomic force microscopy (Fig. 2, right side). The measured period of sinusoidal-like shape was 700 nm and the height (depth of the groove) was 40 nm. In simulations the measured shape of the grating features was approximated by a sine shape. The first type of boundary conditions [Fig. 1(a)] was chosen in simulations. The verification results are based on measured and simulated total reflectance of the structure. The total reflectance was measured with Perkin Elmer Lambda 950 spectrophotometer with unpolarized light, which was considered also in simulations (50% TE +50% TM polarization). In simulations we have used realistic refractive indices of aluminum layer. In Fig. 3, the simulated (dashed curve) and measured (solid curve) total reflectance (R_{tot}) of the grating are presented. Good agreement is observed between the measured and simulated curves of R_{tot}. Both curves show a decrease in R_{tot} at $\lambda \approx 700$ nm, where $\lambda = P$ is fulfilled. According to the grating equation[4] at this condition ($\lambda = P$), the incident light is efficiently scattered in its first scattering order under large scattering angle (close to lateral direction of the grating). This effect leads to pronounced absorption in the Al grating, resulting in a noticeable decrease in R_{tot}. In Fig. 2, the simulation of a flat Al layer is shown in addition, where no such decrease is observed. The verification results of the 2D model on the simple grating (and other grating structures presented elsewhere[13]) indicate that the model is applicable to realistic periodic grating structures.

III. RESULTS OF OPTICAL ANALYSIS AND OPTIMIZATION OF MICROCRYSTALLINE SOLAR CELL

With the developed simulator, we carried out optical analysis and optimization of a thin microcrystalline silicon (μc-Si:H) single-junction solar cell with integrated grating interfaces. The structure of the cell, starting from front layer, is ITO (70 nm)/p-μc-Si:H (15 nm)/i-μc-Si:H (500 nm)/n-μc-Si:H (20 nm)/ZnO (100 nm)/Ag on a substrate with periodic texture. In the simulations, it was assumed that the texture of the substrate is transferred to all interfaces of the solar cell. The sine shape of the texture and the first type of boundary conditions [Fig. 1(a)] were chosen in simulations. The number of triangular elements in the simulation domain of the cell depends on applied light wavelength, grating period, height, optical properties, and thickness of the layers in the solar cell. For example, in a structure with the grating of P=600 nm and h=450 nm at the wavelength of 350 nm, around 400.000 triangular elements were used in the analyzed solar cell structure. 400.000 elements give us approximately 200.000 unknowns in the case of linear approximation [Eq. (2)] as elements share their nodes with adjacent elements. This high number of unknowns appears only in the worst case (largest period, largest

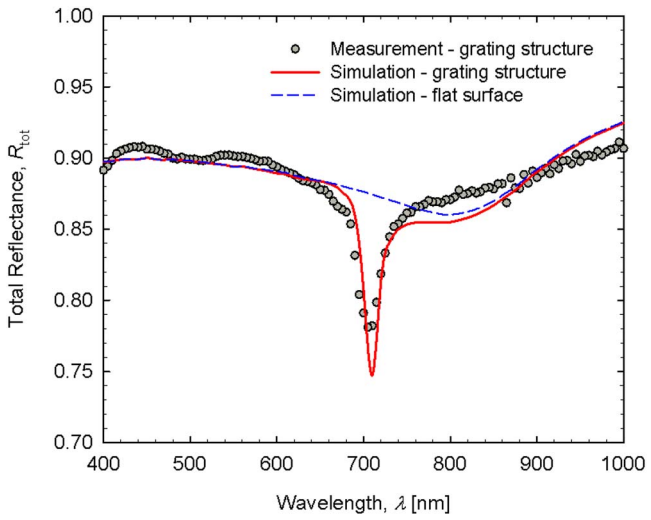

FIG. 3. (Color online) Measured and simulated total reflectance of the aluminum grating structure with P=700 nm and h=40 nm. A simulation of a flat structure (without grating) is shown in addition.

TABLE I. Complex refractive indices $N=n-jk$ (n is the refractive index, and k is the extinction coefficient) for the μc-Si:H layers used in the simulations.

λ (nm)	p-μc-Si:H ($N=n-jk$)	i-μc-Si:H	n-μc-Si:H
400	$4.65-j0.5$	$4.67-j0.45$	$4.69-j0.52$
500	$4.0-j0.123$	$4.1-j0.11$	$4.08-j0.114$
600	$3.75-j0.04$	$3.73-j34.3\times10^{-3}$	$3.79-j0.042$
700	$3.7-j16.5\times10^{-3}$	$3.71-j13.\times10^{-3}$	$3.71-j19.7\times10^{-3}$
800	$3.61-j10.5\times10^{-3}$	$3.65-j5.43\times10^{-3}$	$3.64-j12.1\times10^{-3}$
900	$3.55-j7.55\times10^{-3}$	$3.58-j1.96\times10^{-3}$	$3.57-j9.55\times10^{-3}$
1000	$3.53-j6.53\times10^{-3}$	$3.51-j5.21\times10^{-4}$	$3.51-j8.62\times10^{-3}$

height of the grating, and the smallest wavelength). The smaller the period is, and/or the larger the wavelength, the less elements are required in simulation. However, a sufficient number of elements is required also from the point of view of approximation of the grating shape. In all our simulations (grating with sine shape), we used 40 unknowns per effective wavelength.

Measured wavelength dependent complex refractive indices of materials were used. The values of μc-Si:H layers are summarized in Table I (values given for the wavelength step of 100 nm). The analysis of the cell with respect to P and h of the grating was carried out. The P was changed from 50 to 1500 nm in different discretization steps (see points in the corresponding graphs), while for the h we present the results for $h=150$, 300, and 450 nm. Simplified electrical analysis was used to determine external quantum efficiency (QE) and short-circuit current (J_{SC}) of the cell. In the analysis we assume an ideal extraction of generated charge carriers in the i-μc-Si:H absorber layer and neglect possible contribution of charge carriers from the p- and n-doped layers[14] (close to realistic situation in state-of-the-art μc-Si:H solar cells). In this way, the QE is equal to the absorptance in the intrinsic layer. The J_{SC} is then calculated from QE by applying AM1.5 spectrum ($\lambda=350-1000$ nm). Figure 4 shows the results of J_{SC} of the cell as a function of the P, while h is a parameter. The level of the J_{SC} of the solar cell with flat interfaces is added to the graph (12.16 mA/cm^2).

Simulations indicate a noticeable improvement in J_{SC} of the μc-Si:H cell while increasing the P up to ~600 nm for all h. In this period range local maxima are observed for $h=150$ nm. In the range of $P=600-700$ nm, a maximum of J_{SC} is obtained for all three h. The maximum improvements in J_{SC} for $h=150$, 300, and 450 nm are +40% (+4.87 mA/cm^2), +39% (+4.78 mA/cm^2), and +45% (+5.45 mA/cm^2), respectively, compared to the flat cell. Additional simulations indicated that to achieve 45% improvement in J_{SC} in a cell with flat interfaces, the thickness of the i-μc-Si:H absorber layer should be increased from 500 to 1400 nm (2.8 times thicker). In Fig. 4, for the gratings with higher h the shift of maximum toward larger periods can be observed. Simulations indicated that for $h>450$ nm even higher improvements in the J_{SC} are obtained; however, one should point out that the grating structures with a high aspect ratio ($h/P>2$) are very difficult to fabricate. For the P

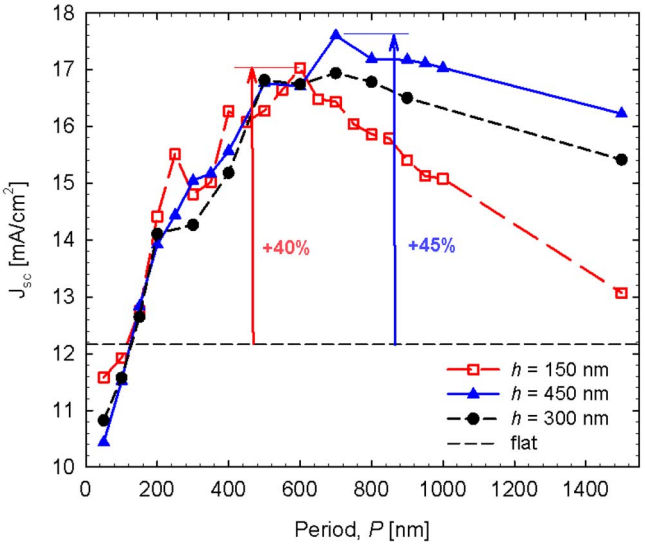

FIG. 4. (Color online) Simulated short-circuit current densities of μc-Si:H cell with sinusoidal periodic texture applied to all interfaces. The effect of changing the period and height of grating structure is shown in comparison to a solar cell with flat interfaces. Simulated points are presented by symbols, where lines are added as a guide for the eyes.

>700 nm, the improvement in J_{SC} starts to decrease. However, the decrease is slower for the cells with large h. Thus, for large P, large h is important.

In the case of using a thicker absorber layer, the J_{SC} increases related to the diffraction gratings are lower (e.g., for an 800 nm thick absorber the increase of 32% is calculated for the grating with $P=700$ nm and $h=450$ nm). However, thinning down the absorber layer is important (and thus efficient light scattering) in order to decrease deposition time of the μc-Si:H layers as well as to reduce material consumption.

In Fig. 5 the calculated QEs corresponding to the cells with $P=600$ nm, $h=150$ nm and $P=700$ nm, $h=450$ nm (maxima in J_{SC}) are shown. The QE of a flat cell is added as

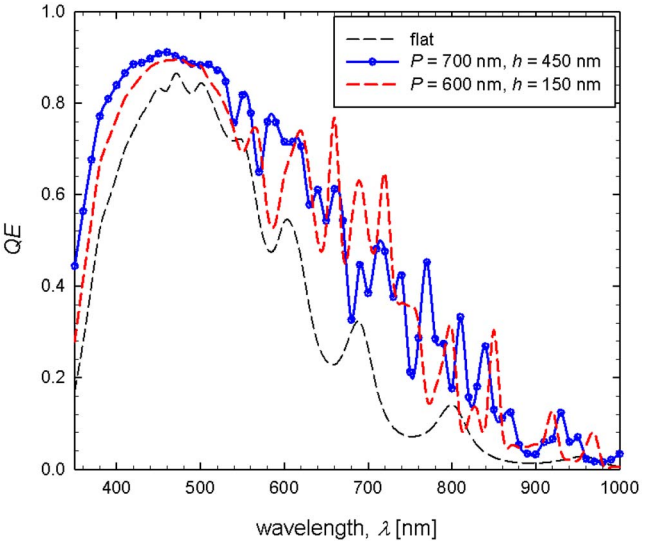

FIG. 5. (Color online) Simulated QE of the μc-Si:H cell with two different combinations of the grating parameters. Simulation of the cell with flat interfaces is plotted for comparison.

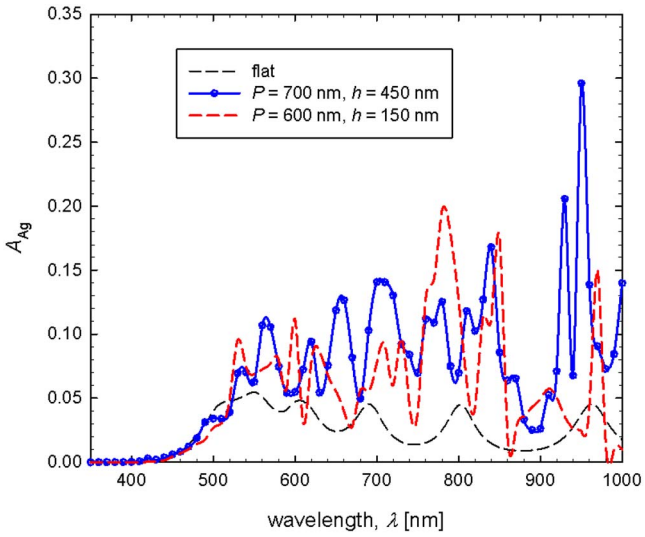

FIG. 6. (Color online) Simulated absorption in the Ag contact in the μc-Si:H solar cells with two combinations of the grating parameters and for the solar cell with flat interfaces.

a reference. The QEs of the cells with the gratings are higher than those for the cells with flat interfaces over the whole wavelength region. Pronounced interferences are observed (at different positions related to different P), indicating significant wavelength-dependent optical behavior of grating texture. Simulations showed that the overall increase in QE is dictated by three main effects: (i) antireflective effect, (ii) improved light scattering, and (iii) optical losses in the metal contact (Ag). Effect (i) increases the transmission of the incident light due to the antireflecting properties of the grating texture at the front interfaces (air/ITO, ITO/p-layer and p-layer/absorber) into absorber layer and improves the QE in whole wavelength region. Effect (ii) is related to efficient scattering of light at the front and rear interfaces of the solar cell. This effect is improving only the long-wavelength QE ($\lambda > 600$ nm), since the short-wavelength light is absorbed already without scattering (for short wavelengths the absorption coefficient of μc-Si:H material is high). By texturing metal interfaces (ZnO/Ag in our case) surface plasmon absorption starts to play a role.[15] The reflectance of the metal interface is reduced due to this parasitic absorption, which might noticeably reduce the long-wavelength QE. This effect (iii) is also included in our simulation. However, the simulator enables to quantify this absorption in the textured Ag. The results of the absorptance in the Ag layer inside the solar cell structure are presented in Fig. 6 for the same gratings as used in the analyzed solar cell. Interference fringes are observed. Significant enhancement in the long-wavelength region can be observed for both types of gratings, compared to the flat Ag. The losses in Ag can be justified in terms of J_{SC} (how much of J_{SC} is lost in Ag). These losses are 2.73, 2.21, and 0.97 mA/cm^2 for the cells with $P=700$ nm and $h=450$ nm, $P=600$ nm and $h=150$ nm, and flat interfaces, respectively. Thus, the increases in the short-circuit current losses in Ag related to the texturing of the interfaces in the cell are 180% and 130% with respect to the cell with flat interfaces.

IV. CONCLUSIONS

The 2D optical simulator for simulation of thin-film solar cells with periodically textured interfaces was presented. The optical model is based on robust FEM method of solving Maxwell equation. Both TE and TM polarizations of light are included. Boundary conditions and how to effectively solve the system of discretized differential equations were presented. The advantages of the described modeling approach were highlighted.

The simulator was verified on Al/polycarbonate grating structure with a period of 700 nm and a height of 40 nm. The result of optical analysis and optimization of a complete microcrystalline silicon solar cell with different periods and heights of the incorporated sinusoidal grating is presented. For the selected i-μc-Si:H solar cell, the optimal values for period and height are determined to be $P \approx 700$ nm and $h \approx 450$ nm. Up to 45% (+5.45 mA/cm^2) improvement in J_{SC} of the solar cell is predicted for the cell with optimized grating, compared to the same cell with flat interfaces. Additional absorption in textured Ag metal layer was quantified. The developed 2D optical simulator presents a powerful tool for further investigation of light management in thin-film solar cell with the periodic diffractive gratings and textures of other shapes.

ACKNOWLEDGMENTS

The authors thank Miro Zeman from DIMES, Delft University of Technology, The Netherlands for providing the grating sample and for useful discussions on optical modeling, and OM&T B.V., The Netherlands for providing polycarbonate substrates.

[1] J. Müller, B. Rech, J. Springer, and M. Vanecek, Sol. Energy **77**, 917 (2004).
[2] S. Faÿ, S. Dubail, U. Kroll, J. Meier, Y. Ziegler, and A. Shah, Proceedings of the 16th EU PVSEC, Glasgow, 2000 (unpublished), p. 361.
[3] M. Kambe, M. Fukawa, N. Taneda, Y. Yoshikawa, K. Sato, K. Ohki, S. Hiza, A. Yamada, and M. Konagai, Proceedings of the WCPEC-3, Osaka, 2003 (unpublished), p. 1812.
[4] C. Heine and R. H. Morf, Appl. Opt. **34**, 2476 (1995).
[5] J. Jin, *The Finite Element Method in Electromagnetics*, 2nd ed. (Wiley, New York, 2002).
[6] J. Krč, M. Zeman, A. Čampa, F. Smole, and M. Topič, Proceedings of the MRS 2006 Spring Meeting, San Francisco, CA [Mater. Res. Soc. Symp. Proc. **910**, A25.1.1 (2006)].
[7] S. Cui and D. S. Weile, Microwave Opt. Technol. Lett. **35**, 106 (2002).
[8] S. D. Gedney, J. F. Lee, and R. Mittra, IEEE Trans. Microwave Theory Tech. **40**, 363 (1992).
[9] W. Ritz, J. Reine Angew. Math.. **135**, 1 (1908).
[10] R. Barrett, M. Berry, T. F. Chan, J. Demmel, J. Donato, J. Dongarra, V. Eijkhout, R. Pozo, C. Romine, and H. Van der Vorst, *Templates for the Solution of Linear Systems*, 2nd ed. (SIAM, Philadelphia, 1994).
[11] Y. Saad, *Iterative Methods for Sparse Linear Systems*, 2nd ed. (SIAM, Philadelphia, 2003).
[12] A. Čampa, J. Krč, and M. Topič, Informacije MIDEM **38**, 5 (2008).
[13] A. Čampa, O. Isabella, R. van Erven, P. Peeters, H. Borg, J. Krc, M. Topic, and M. Zeman, Book of Abstracts MRS 2008 Spring Meeting, 2008 (unpublished); www.mrs.org.
[14] M. Zeman, R. A. C. M. M. van Swaaij, J. W. Metselaar, and R. E. I. Schropp, J. Appl. Phys. **88**, 6436 (2000).
[15] J. Springer, A. Poruba, L. Müllerova, and M. Vanecek, J. Appl. Phys. **95**, 1427 (2004).